ACS Catalysis

Research Article

pubs.acs.org/acscatalysis

# Pd and Pd–Ag Nanoparticles within a Macroreticular Basic Resin: An Efficient Catalyst for Hydrogen Production from Formic Acid Decomposition

Kohsuke Mori,[†,‡] Masahiro Dojo,[†] and Hiromi Yamashita[†,‡,*]

[†]Division of Materials and Manufacturing Science, Graduate School of Engineering, Osaka University, 2-1 Yamada-oka, Suita, Osaka 565-0871, Japan

[‡]ESICB, Kyoto University, Katsura, Kyoto 615-8520, Japan

Supporting Information

**ABSTRACT:** A basic resin bearing $-N(CH_3)_2$ functional groups within its macroreticular structure performed as an efficient organic support for the active Pd nanoparticles (NPs) responsible for the production of high-quality $H_2$ via formic acid (HCOOH) decomposition at convenient temperature. Physicochemical characterization as well as the kinetic isotope effect (KIE) revealed that not only the formation of small Pd NPs but also cooperative action by the $-N(CH_3)_2$ groups within the resins play crucial roles in achieving efficient catalytic performances. In addition to the advantages such as simple workup procedure, free of additives, and superior catalytic activity compared with the conventional inorganic supports, the present catalytic system can suppress unfavorable CO formation of <5 ppm, which makes it an ideal hydrogen vector in terms of potential industrial application for proton-exchange-membrane fuel cells. Moreover, the basic resin support also provides Pd–Ag nanocatalyst from an aqueous solution of mixture of $PdCl_2$ and $AgNO_3$. The catalytic activities in the $H_2$ production from formic acid decomposition were strongly dependent on the presence of Ag atoms and were shown to perform significantly better than the pure Pd and Ag catalysts.

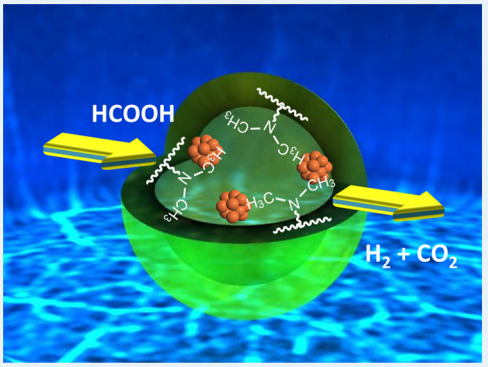


**KEYWORDS:** *palladium, basic resin, hydrogen production, formic acid decomposition, Pd–Ag bimetal*

## 1. INTRODUCTION

Hydrogen has received increasing attention in industry as a candidate for clean energy because the only byproduct of its reaction with oxygen is water,[1] and very efficient energy conversion can be realized by combining with proton exchange membrane fuel cell (PEMFC) technology.[2,3] However, the widespread application of hydrogen as a transportation fuel is limited, mainly because of controllable storage and delivery problems. A considerable amount of research effort is currently devoted to exploring new storage methods, including the use of metal hydrides,[4,5] carbon nanostructures,[6] and metal–organic frameworks.[7,8] Formic acid (HCOOH), which is a liquid at room temperature and contains 4.4 wt % hydrogen, is one of the major products formed during biomass processing and is widely recognized as a nontoxic and convenient hydrogen carrier for fuel cells designed for portable use.[9−11] Formic acid decomposition occurs by two different pathways, through either dehydrogenation (eq 1) or dehydration (eq 2). Selective dehydrogenation is indispensable for the production of ultrapure $H_2$ without undesirable dehydration, since toxic CO contamination produced by the latter pathway significantly reduces the activity of Pt catalysts in fuel cells.

$$HCOOH \rightarrow H_2 + CO_2 \quad \Delta G = -48.4\ kJ{\cdot}mol^{-1} \qquad (1)$$

$$HCOOH \rightarrow H_2O + CO \quad \Delta G = -28.5\ kJ{\cdot}mol^{-1} \qquad (2)$$

Recently, there have been reports of effective decomposition of formic acid using homogeneous catalysts at ambient temperatures.[12−15] Nevertheless, the use of metal complexes combined with excess amine leads to severe difficulties in device fabrication due to separation issues. In this context, current research has been focused on the development of practical heterogeneous catalysts that exhibit significant activity under convenient conditions. Although some progress has been achieved,[16−24] such catalysts often suffer as a result of a need for additives, harsh reaction conditions, and poor selectivity. It is expected that the exploitation of novel catalytic systems may facilitate their widespread application in fuels cells for small portable electronic devices.

Functional resins have been widely utilized in fundamental academic research and industrial applications.[25] The unique surface properties of such resins, including their hydrophilic/hydrophobic characteristics, the ease of introduction of a range of functional groups, and their ability to swell in a reaction

Received: February 25, 2013
Revised: April 1, 2013
Published: April 15, 2013

   dx.doi.org/10.1021/cs400148n | ACS Catal. 2013, 3, 1114–1119

**Table 1. Textural Properties of Resin Supported Pd Resin Catalysts**

| catalyst | resin[a] | functional group | exchange capacity (meq/mL) | property | water absorption capacity (%) | av Pd size (nm)[b] |
|---|---|---|---|---|---|---|
| Pd/resin **1** | 200CTNa | $-SO_3H$ | ≥1.8 | strongly acidic | 46−51 | 5.1 |
| Pd/resin **2** | FPC3500 | −COOH | ≥2.0 | weakly acidic | 60−70 | 2.1 |
| Pd/resin **3** | IRA96SB | $-NMe_2$ | ≥1.3 | weakly basic | 57−63 | 1.7 |
| Pd/resin **4** | IRA900JCl | $-NMe_3Cl$ | ≥1.0 | strongly basic | 56−65 | 5.8 |

[a]Styrenic matrix except for resin **2** (acrylic). [b]Determined from TEM image.

medium, make these materials very attractive from the viewpoint of catalyst design.[26] Moreover, these resins can be used to stabilize highly dispersed metal nanoparticles (NPs) inside macroreticular domains with controllable morphology, along with reasonable thermal and mechanical stability, offering promising catalyst support for a number of industrial processes. It is well-known that the existence of suitable surface functional groups in the vicinity of active metal centers exerts an advantageous influence on catalytic activity. In addition, swelling properties can result in dramatic improvements in the accessibility of reactants in the liquid phase. Consequently, catalytically active species generated within a functional resin matrix essentially differ from conventional solid supported metal catalysts.[27]

In this study, we successfully utilized a basic resin as a platform for hydrogen production from formic acid decomposition, in which cooperative action between active Pd NPs and weakly basic $-N(CH_3)_2$ groups within the resin played an important role in achieving efficient catalytic performance. The catalytic system described here is a promising candidate for a powerful protocol for formic acid decomposition because it has the following advantages: (i) no requirement for additives, (ii) superior catalytic activity compared with conventional inorganic supports, (iii) suppression of concomitant CO formation (to a level of <5 ppm), and (iv) the formation of Pd−Ag nanocatalyst significantly enhanced the catalytic activity.

## 2. RESULTS AND DISCUSSION

**2.1. Pd Nanocatalyst.** Several Pd catalysts were prepared from commercially available resins (Amberlite, Rohm and Haas) with different chemical properties. The characteristics of the resins are summarized in Table 1. Resin 200CTNa (resin **1**) is strongly acidic, and FPC3500 (resin **2**) is weakly acidic, whereas IRA96SB (resin **3**) and IRA900JCl (resin **4**) are weakly and strongly basic, respectively. All of the resins showed moderate BET-specific surface areas of ∼45 $m^2\ g^{-1}$. Pd deposition was carried out by a simple ion exchange procedure using a $PdCl_2$ solution in aqueous HCl. After deposition, the resins were crushed by a ball mill. Subsequently, the samples were reduced with $NaBH_4$. The resulting catalysts are denoted Pd/resins **1**−**4**.

Figure 1A shows Pd K-edge X-ray absorption near edge structure (XANES) spectra before and after reduction for Pd/resins **1** and **3**, together with $PdCl_2$ and Pd foil as reference samples. The shapes of the XANES spectra and the edge positions of the as-synthesized Pd/resins (c and d) were identical to those of $PdCl_2$ (a) but differed from those of Pd foil (b), thus revealing that most of the Pd species were in the II oxidation state. The FT-EXAFS data are shown in Figure 1B. The Pd species entrapped within the acidic resin **1** exhibited a main peak due to the Pd−O bond at around 1.5 Å, corresponding to interaction of the $Pd^{II}$ ions with the $-SO_3^-$ groups of the resin matrix (c). In contrast, the basic Pd/resin **3** (d) exhibited only a peak due to a Pd−Cl bond at around 1.9 Å,

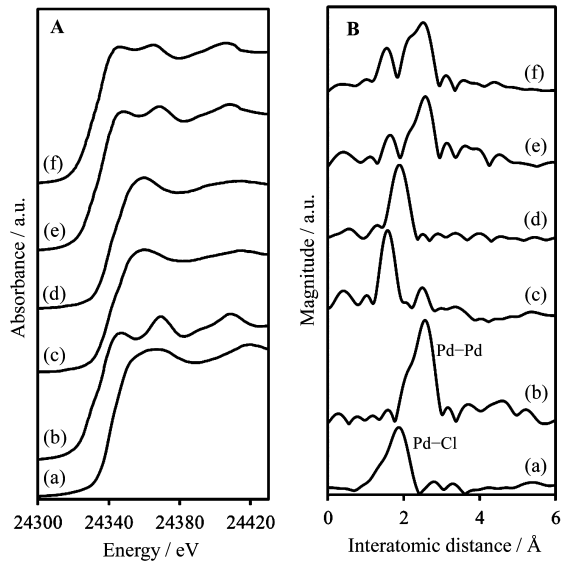


**Figure 1.** (A) Pd K-edge XANES spectra and (B) FT-EXAFS spectra for (a) $PdCl_2$, (b) Pd foil, (c) as-synthesized Pd/resin **1**, (d) as-synthesized Pd/resin **3**, (e) Pd/resin **1** after reduction with $NaBH_4$, and (f) Pd/resin **3** after reduction with $NaBH_4$.

indicating that the $Pd^{II}$ species may exist in this case as monomeric $[PdCl_4]^{2-}$.

As shown in Figure 1A, the Pd K-edge XANES spectra (e and f) for the reduced Pd/resins were similar to that for the Pd foil (b). The FT-EXAFS spectra exhibited a main peak at ∼2.5 Å due to Pd−Pd bonds found in the metal (e and f), together with an additional small peak due to a Pd−O bond in the first coordination sphere. The XRD pattern did not show any distinct peaks characteristic of the PdO and fcc Pd lattice, suggesting that small Pd nanoparticles (NPs) were formed within the reticular domain of the resins. The edge position (measured at the half-height of the edge jump) in the Pd K-edge XANES spectrum depends on the electronic charge of the Pd species. Closer inspection indicates that the energy of Pd/resin **3** is slightly lower than those of the Pd/resin**1** and Pd foil (∼1 eV, Supporting Information Figure S2), suggesting that the weakly basic $-N(CH_3)_2$ groups may have an electron-donating effect.[28] The formation of Pd NPs can also be confirmed by the transmission electron microscopy (TEM) analysis, in which relatively small Pd NPs with a narrow size distribution were observed. A typical TEM image and size distribution histogram for the basic resin **3** are shown in Supporting Information Figure S1, as a representative result. As summarized in Table 1, the mean diameters of the Pd NPs in Pd/resins **1**−**4** were determined to be 5.1, 2.1, 1.7, and 5.8 nm, respectively, suggesting that the size of the Pd NPs was influenced by the properties of the resin supports. As mentioned before, Pd K-edge XAFS analysis revealed that the Pd species entrapped within the acidic resin **1** exist as $Pd^{II}$ ions surrounded by the


dx.doi.org/10.1021/cs400148n | ACS Catal. 2013, 3, 1114−1119

$-SO_3^-$ groups of the resin matrix, whereas the $Pd^{II}$ species exist as monomeric $[PdCl_4]^{2-}$ in the case of the basic resin **3** with basic $-N(CH_3)_2$ groups. It can be said that the different property of the resin supports generate the different Pd precursors, which may influence the formation of nuclei of metals as well as the consecutive growth and, finally, produce different sizes of Pd NPs. These results suggest that the present methodology would be a convenient approach to control the size of Pd NPs by varying the kind of resins because of simplicity and reproducibility.

To evaluate their catalytic ability, the Pd/resins were used for hydrogen production from formic acid decomposition in a closed liquid-phase system. The results are summarized in Figure 2, together with the average diameter of the Pd NPs.

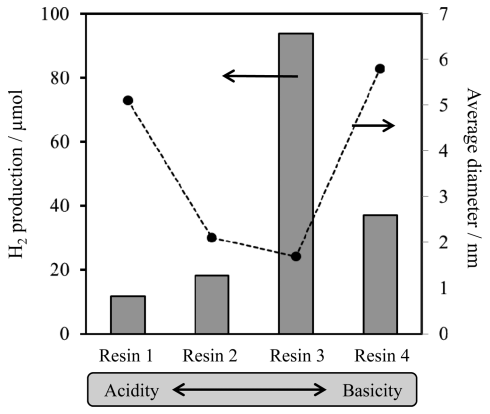


**Figure 2.** Relationship between $H_2$ production and average diameter of Pd NPs for various resins.

Pd/resin **3**, with weakly basic $-N(CH_3)_2$ groups, exhibited the highest activity among those examined, with $H_2$ productivity reaching 96 $\mu$mol. No induction period was observed, and the ratios of $H_2$ to $CO_2$ generated during the course of the reaction were almost 1 for all samples. The catalytic activity was greatly influenced by the properties of resins, decreasing in the following order: Pd/resin **3** (weakly basic) > Pd/resin **4** (strong basic) > Pd/resin **2** (weakly acidic) > Pd/resin **1** (strongly acidic). The average diameter of the Pd NPs in the most active Pd/resin **3**, was 1.7 nm, which was smaller than those for the other Pd/resins. This result suggested that the formation of small Pd NPs might be a simple explanation for the high catalytic activity of Pd resin **3**. However, the weakly acidic Pd/resin **2** showed low activity, despite its relatively small average Pd NP diameter of 2.1 nm, whereas the strongly basic resin **4** showed moderate activity despite the relatively large average diameter of its Pd NPs (5.8 nm). Accordingly, it is supposed that not only the size of the Pd NPs but also the properties of the resin were important factors in attaining high catalytic activity.

Notably, the catalytic activity of Pd/resin **3** was significantly higher than those of our prepared conventional catalysts with the same Pd content. Figure 3 shows $H_2$ production based on the electronegativity of various inorganic support metals. The average mean diameter of Pd NPs, as determined by CO adsorption, ranged from 3.4 to 4.7 nm. The use of basic $CeO_2$, which has low electronegativity, resulted in poor activity, whereas MgO and $ZrO_2$, which are weakly basic, showed moderate activity. As expected, the catalytic activity of $Al_2O_3$ and $TiO_2$ decreased with increasing electronegativity. The

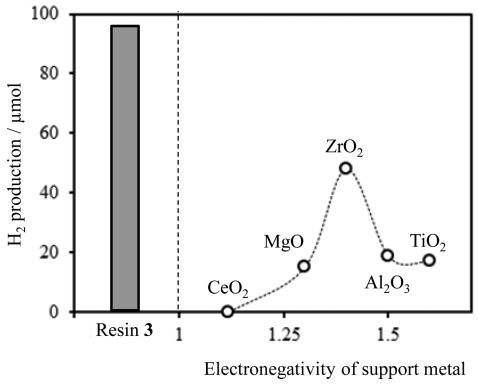


**Figure 3.** $H_2$ production for various Pd-supported catalysts with different electronegativities.

importance of the macroreticular structure in combination with weak basicity was also demonstrated by the above results.

Significantly, the applicability of the present catalyst was highlighted by the open system reaction equipped with gas buret at 348 K using an HCOOH/HCOONa = 9/1 aqueous solusion, in which the reaction rate approached 2880 mL $min^{-1}$ $g^{-1}$(Pd) with a high TOF 820 $h^{-1}$. It is noteworthy that this TOF value achieved by the Pd/resin is higher than those reported for other active catalyst systems, such as Pd–Au/C (27 $h^{-1}$, 365 K),[16] Pd/C (255 $h^{-1}$, 373 K),[18] $Mo_2C$/C Pd–Au/C (437 $h^{-1}$, 423 K),[19] and Ag@Pd/C (626 $h^{-1}$, 363 K).[21] Moreover, the catalytic system under discussion suppressed unfavorable CO contamination from the dehydration pathway, with <5 ppm of CO present during the course of the reaction, as shown in Supporting Information Figure S3. This concentration was significantly lower than that obtained by conventional gas reforming from $CH_3OH$, $C_2H_5OH$, and $CH_4$ and meets the criteria of the PEMFC standard, which is a CO concentration lower than 10 ppm.[29,30] Furthermore, the present catalyst almost keeps its original catalytic activity, even after the recycling experiments. The reaction using the filtrate after the removal of catalyst did not show any catalytic activity, suggesting no leaching of active Pd species. This catalytic system is a promising candidate for an ideal hydrogen vector in terms of potential industrial application for PEMFCs.

As mentioned before, the dehydrogenation reaction occurred exclusively to give $H_2$ and $CO_2$ in a molar ratio of 1:1 without the formation of CO by dehydration. The decomposition of HCOOH was promoted in the presence of basic supports. Moreover, the preliminary results described below were observed; the IR spectrum of Pd/resin **3**, upon treatment with formic acid, showed a shift of the $\nu$(C=O) band toward 1695 $cm^{-1}$, in comparison with the free carbonyl group at 1725 $cm^{-1}$ (Supporting Information Figure S4). The addition of HCOONa to the reaction mixture significantly increased $H_2$ productivity (Supporting Information Figure S5). These results indicated the participation of the Pd–formate species as a reaction intermediate. Upon consideration of the above results, we deduced a possible reaction pathway on the surface of $Pd^0$ NPs within the basic resin, which is illustrated in Scheme 1.[31] First, O–H bond cleavage is facilitated with the assistance of the weakly basic $-N(CH_3)_2$ group as a proton scavenger, affording a paladium formate species along with a $-^+HN(CH_3)_2$ group. The paladium formate species may undergo $\beta$-hydride elimination to produce $CO_2$ and a paladium hydride species. The reaction of the hydride species with $-^+HN(CH_3)_2$


dx.doi.org/10.1021/cs400148n | ACS Catal. 2013, 3, 1114–1119

**Scheme 1. A Possible Reaction Pathway for the $H_2$ Production from Formic Acid Decomposition by the Pd/resin 3 with Basic Group**

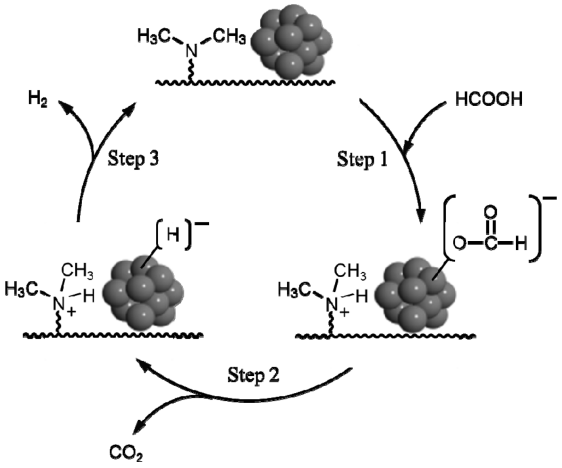


produces molecular hydrogen, along with regeneration of the $Pd^0$ species.

The results for kinetic isotope effect (KIE) using HCOOH, HCOOD, and DCOOH are summarized in Table 2. The $k_H/k_D$ values obtained from both competitive reactions using the basic Pd/resin **3** were smaller than those obtained using acidic Pd/resin **1**. This is clear evidence that the basic $-N(CH_3)_2$ groups have a positive effect on O−H bond dissociation, which is subsequently associated with rate-determining C−H bond cleavage from the Pd−formate intermediate to release $H_2$. It has been reported that high catalytic activity can be obtained for formic acid decomposition in the presence of amine in both homogeneous and heterogeneous systems.[15,24] It is reasonable to conclude that cooperative action by the amine functionality within the macroreticular resin accounts for its high catalytic activity.

**Table 2. KIE in the Decomposition of Formic Acid**

| catalyst | formic acid | reaction rate ($\mu$mol•min$^{-1}$) | $k_H/k_D$ |
|---|---|---|---|
| Pd/resin **1** (strongly acidic) | HCOOH | 0.084 | |
| | HCOOD | 0.049 | 1.71 |
| | DCOOH | 0.032 | 2.63 |
| Pd/resin **3** (weakly basic) | HCOOH | 2.83 | |
| | HCOOD | 2.41 | 1.17 |
| | DCOOH | 1.43 | 1.98 |
| Pd−Ag/resin **3** (weakly basic) | HCOOH | 2.36 | |
| | HCOOD | 2.28 | 1.04 |
| | DCOOH | 1.38 | 1.65 |

**2.2. Pd−Ag Nanocatalyst.** The development of bimetallic nanoparticle catalysts has attracted recent attention as a result of their improved catalytic activity and selectivity resulting from the architectural configuration of two metals as alloys or with core−shell structure.[32] We attempted the deposition of both Pd and Ag within the basic resin **3** to form Pd−Ag nanocatalysts by a simple ion exchange method from an aqueous solution of $PdCl_2$ and $AgNO_3$ with different molar ratios. Subsequently, the samples were reduced with $NaBH_4$. From the TEM image, the average particle size of Pd−Ag nanocatalysts increased with an increase in the amount of Ag loading: 3.2 nm (Pd/Ag = 1:1) < 9.8 nm (Pd/Ag = 1:2) < 10.4 nm (Pd/Ag = 1:3) ≈ 10.5 nm (Pd/Ag = 1:4) (Supporting Information Figure S6). XAFS measurements were carried out to elucidate the structure of the Pd−Ag nanocatalysts (Figure 4). The Pd K-edge FT-EXAFS spectra of Pd−Ag/resin **3** exhibited two peaks due to the Pd−O bond at ∼1.5 Å and the contiguous Pd−Pd bond in the metallic form. The Pd−Pd distance, however, was found to be shifted to a slightly longer interatomic distance when compared with pure Pd foil, and a more significant shift can be observed with an increase in the amount of Ag. This indicates the presence of heteroatomic bonding in the Pd−Ag nanocatalyst. In the Ag K-edge FT-EXAFS spectra, Pd−Ag nanocatalysts and the reference Ag foil showed intense singlet peak at around 2.6 Å, which was ascribed to the nearest metal−metal bonding, which was slightly shifted to a shorter interatomic distance when compared with pure Ag foil with an increase in the amount of Ag. This result also suggests the formation of heteroatomic Pd−Ag bonding. For the structural model of the Pd−Ag nanocatalysts, it is reasonable to suggest that the Ag atoms are preferentially located in the core region, whereas the Pd atoms are preferentially located in the shell region, since EXAFS analysis revealed that the Pd atoms exist in a more oxidized state than Ag atoms because of the exposure to the surface. The above speculation was supported by the catalytic results, as will be shown later.

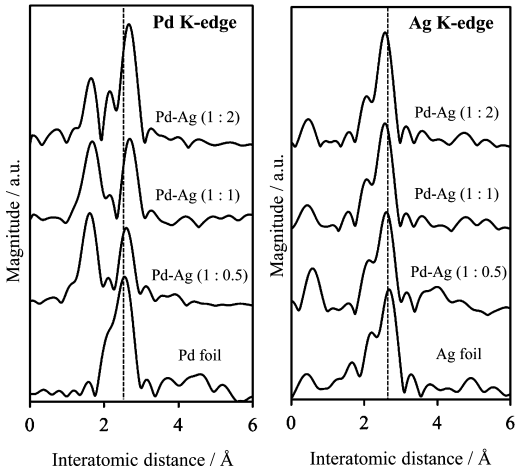


**Figure 4.** Pd and Ag K-edge FT-EXAFS spectra of Pd−Ag/resin **3** with different Pd and Ag ratios and foil references.

Figure 5 shows the comparison of the catalytic activities of the Pd−Ag resins with different Pd and Ag molar ratios. The Pd−Ag (1:2)/resin **3** catalyst performed significantly better than the pure Pd catalyst. The reaction using pure Ag catalyst hardly occurred. The enhancement effect was almost negligible when the physical mixture of pure Pd and Ag catalysts was employed. These results indicate that a synergic effect exists between Pd and Ag atoms for the basic resin-supported catalysts. Remarkably, the open system reaction equipped with a gas buret at 348 K using HCOOH/HCOONa = 9/1 aqueous solusion gives a high reaction rate of more than 6000 mL $min^{-1}$ $g^{-1}$ (Pd) with high TOF 1900 $h^{-1}$ based on Pd. Assuming 50% fuel cell effciency, this reforming gas output correspnds to a theoretical power density of approximately 200 W $h^{-1}$ $g^{-1}$(Pd) for energy generation.[10]

Recently, there have been reports dealing with Pd−Ag catalysts for the decomposition of formic acid. For example, Tsang et al. demonstrated that the use of core−shell type Pd−


dx.doi.org/10.1021/cs400148n | ACS Catal. 2013, 3, 1114−1119

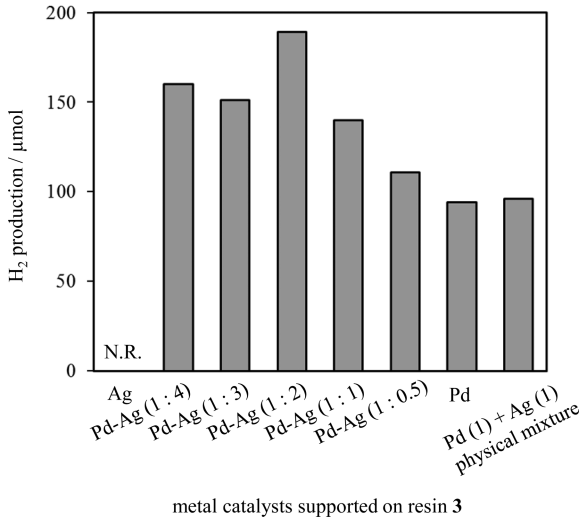


**Figure 5.** Effect of the addition of Ag on the $H_2$ production.

Ag nanocatalysts supported on carbon led to high yields of $H_2$.[21] Xian and co-workers reported that the addition of Ag to Pd significantly improves the efficiency of $H_2$ formation and that a high productivity is realized using carbon or $CeO_2(H_2O)_x$ as a support.[16] It has been supposed that the activity of formic acid decomposition is related to the intrinsic electronic properties of the metallic particles: the closer the d band center is to the Fermi level of a metal, the higher the adsorption energy of the formic acid.[33] Thus Pd atoms exhibit a higher activity than Ag atoms. In the case of the core−shell Pd−Ag nanocatalysts, the charge transfer from Ag core to the Pd shell owing to the net difference in work function strengthens the adsorption of formate through strong back-donation and, finally, enhance the rate of $H_2$ production. As shown in Table 2, the $k_H/k_D$ values obtained from KIE analysis using the Pd−Ag/resin **3** were smaller than those obtained using pure Pd/resin **3**. This result indicates that the Pd−Ag nanocatalyst facilitates O−H bond dissociation of formic acid as well as rate-determining C−H bond cleavage from the Pd−formate intermediate. Another explanation for the enhancement of catalytic activity by the addition of Ag may be the efficient inhibition of CO adsorption compared wiht the pure Pd metals,[34,35] which consequently prolong the lifetime of the catalyst.

## 3. CONCLUSION

In summary, we have demonstrated that the basic resin bearing $-N(CH_3)_2$ functional groups within its macroreticular structure act as a promising support to produce active Pd catalyst for the production of $H_2$ from formic acid decomposition. The basicity of the resins and the smaller size of the Pd NPs are found to be key factors in achieving efficient catalytic performances at a convenient temperature. The deposition of both Pd and Ag to form Pd−Ag nanocatalyst was also accomplished, which showed an enhancement in the catalytic efficiency of $H_2$ production. The features of the present catalytic system, such as facile preparation, free of additives, and superior catalytic activity compared with conventional inorganic supports as well as suppression of unfavorable CO formation to a level of <5 ppm are particularly desirable for industrial application as a hydrogen vector for the portable PEMFCs.

## EXPERIMENTAL SECTION

**Materials.** $PdCl_2$ was purchased from Wako Pure Chemical Ind., Ltd. All resins were Amberlite, supplied by Rohm and Haas. Metal oxides were kindly supplied by the Japan Catalysis Society. Solvents and all commercially available organic compounds for catalytic reactions were used as received.

**Synthesis of Pd Catalyst.** Several Pd catalysts were prepared from commercially available resins (Amberlite, Rohm and Haas) with different chemical properties. A suspension containing the resin (5.0 g) and 200 mL of the aqueous $PdCl_2$ solution ($11.3 \times 10^{-4}$ M) was stirred at room temperature for 24 h. The mixture was filtered, and the solid obtained was washed repeatedly with distilled water and air-dried overnight. After the deposition, the resins were crushed by a ball mill (600 rpm for 10 min). Subsequently, the samples were prereduced with $NaBH_4$ to give Pd/resin catalyst. Induction coupled plasma (ICP) analysis determined that the Pd species were easily attached to the resins at the same level of loading (Pd: 0.5 wt %). $Pd/TiO_2$ (rutile), $Pd/ZrO_2$, $Pd/CeO_2$, Pd/MgO, and $Pd/Al_2O_3$ (Pd: 0.5 wt %) were also prepared by the conventional impregnation method using an aqueous solution of $PdCl_2$. The resulting material was centrifuged, washed repeatedly with deionized water, and dried under vacuum. The synthesized sample was calcined at 823 K for 5 h and treated with $NaBH_4$.

**Synthesis of Pd−Ag Nanocatalyst.** A suspension containing the resin (5.0 g) and 200 mL aqueous $PdCl_2$ solution ($11.3 \times 10^{-4}$ M) and $AgNO_3$ t different molar ratios was stirred at room temperature for 24 h. The mixture was filtered, and the solid obtained was washed repeatedly with distilled water and air-dried overnight. After the deposition, resins were crushed by a ball mill (600 rpm for 10 min). Subsequently, the samples were prereduced with $NaBH_4$, giving Pd−Ag nanocatalysts with different molar ratios (Pd/Ag = 1:0.5, 1:1, 1:2, 1:3, 1:4).

**Characterization.** Powder X-ray diffraction patterns were recorded using a Rigaku RINT2500 diffractometer with Cu K$\alpha$ radiation ($\lambda$ = 1.5406 Å). BET surface area measurements were performed using a BEL-SORP max (Bel Japan, Inc.) at 77 K. The sample was degassed in vacuum at 373 K for 2 h prior to data collection. Inductively coupled plasma optical emission spectrometry (ICP-OES) measurements were performed using a Nippon Jarrell-Ash ICAP-575 Mark II. Infrared spectra were obtained with a JASCO FTIR-6100. Samples were diluted with KBr and compressed into thin disk-shaped pellets. TEM micrographs were obtained with a Hitachi Hf-2000 FE-TEM equipped with a Kevex energy-dispersive X-ray detector operated at 200 kV. Pd K-edge and Ag K-edge XAFS spectra were recorded using a fluorescence−yield collection technique at the beamline 01B1 station with an attached Si (311) monochromator at SPring-8, JASRI, Harima, Japan (Prop. No. 2011B1107, 2012A1061). The EXAFS data were normalized by fitting the background absorption coefficient, around the energy region higher than that of the edge of about 35−50 eV, with smooth absorption of an isolated atom. The EXAFS data were examined using the Rigaku EXAFS analysis program. Fourier transformation (FT) of $k^3$-weighted normalized EXAFS data was performed over the 3.5 Å < $k$/Å$^{-1}$ < 11 Å range to obtain the radial structure function.

**Decomposition of Formic Acid.** In the case of the closed system, the resin catalyst (0.05 g) was placed into a reaction vessel (30 mL) containing $H_2O$ (9.6 mL), which was then


dx.doi.org/10.1021/cs400148n | ACS Catal. 2013, 3, 1114−1119

sealed with a rubber septum. The resulting mixture was bubbled with Ar for 15 min, followed by the addition of HCOOH (0.39 mL), and subsequently reacted with magnetic stirring at 337 K. The progress of the reaction was monitored by a Shimadzu GC-14B equipped with MS5 Å columns for $H_2$ and porapakQ for $CO_2$. In the case of the open system reaction, the catalyst was placed into a reaction vessel (30 mL) with a reflux condenser and equipped with gas buret. After purging with Ar, HCOOH/HCOONa = 9/1 aqueous solusion (1M, 10 mL) was added to the reaction vessel and reacted at 348 K with with magnetic stirring.

## ■ ASSOCIATED CONTENT

### Supporting Information

TEM images and FT-IR spectra. This material is available free of charge via the Internet at http://pubs.acs.org.

## ■ AUTHOR INFORMATION

### Corresponding Author

*Phone, Fax: +81-6-6879-7457. E-mail: yamashita@mat.eng.osaka-u.ac.jp.

### Notes

The authors declare no competing financial interest.

## ■ ACKNOWLEDGMENTS

The present work was partially supported by MEXT program "Elements Strategy Initiative to Form Core Research Center", MEXT, Ministry of Education Culture, Sports, Science, and Technology, Japan. We acknowledge Dr. Eiji Taguchi and Prof. H. Yasuda at the Research Center for Ultra-High Voltage Electron Microscopy, Osaka University, for their assistance with the TEM measurements. XAFS spectra were recorded at the beamline 01B1 station in SPring-8, JASRI, Harima, Japan (Prop. No. 2011B1107, 2012A1061).

## ■ REFERENCES

(1) Park, S.; Vohs, J. M.; Gorte, R. J. *Nature* **2000**, *404*, 265−267.
(2) Costamagna, P.; Srinivasan, S. *J. Power Sources* **2001**, *102*, 242−252.
(3) Steele, B. C. H.; Heinzel, A. *Nature* **2001**, *414*, 345−352.
(4) Schuth, F.; Bogdanovic, B.; Felderhoff, M. *Chem. Commun.* **2004**, *0*, 2249−2258.
(5) Filinchuk, Y.; Chernyshov, D.; Nevidomskyy, A.; Dmitriev, V. *Angew. Chem. Int. Ed.* **2008**, *47*, 529−532.
(6) Bünger, U.; Zittel, W. *Appl. Phys. A: Mater. Sci. Process.* **2001**, *72*, 147−151.
(7) Rosi, N. L.; Eckert, J.; Eddaoudi, M.; Vodak, D. T.; Kim, J.; O'Keeffe, M.; Yaghi, O. M. *Science* **2003**, *300*, 1127−1129.
(8) Li, Y.; Yang, R. T. *J. Am. Chem. Soc.* **2005**, *128*, 726−727.
(9) Joó, F. *ChemSusChem* **2008**, *1*, 805−808.
(10) Grasemann, M.; Laurenczy, G. *Energy Environ. Sci.* **2012**, *5*, 8171−8181.
(11) Enthaler, S.; von Langermann, J.; Schmidt, T. *Energy Environ. Sci.* **2010**, *3*, 1207−1217.
(12) Loges, B.; Boddien, A.; Junge, H.; Beller, M. *Angew. Chem. Int. Ed.* **2008**, *47*, 3962−3965.
(13) Himeda, Y. *Green Chem.* **2009**, *11*, 2018−2022.
(14) Boddien, A.; Loges, B.; Junge, H.; Gärtner, F.; Noyes, J. R.; Beller, M. *Adv. Synth. Catal.* **2009**, *351*, 2517−2520.
(15) Loges, B.; Boddien, A.; Gärtner, F.; Junge, H.; Beller, M. *Top. Catal.* **2010**, *53*, 902−914.
(16) Zhou, X.; Huang, Y.; Xing, W.; Liu, C.; Liao, J.; Lu, T. *Chem. Commun.* **2008**, *0*, 3540−3542.
(17) Ojeda, M.; Iglesia, E. *Angew. Chem. Int. Ed.* **2009**, *48*, 4800−4803.
(18) Bulushev, D. A.; Beloshapkin, S.; Ross, J. R. H. *Catal. Today* **2010**, *154*, 7−12.
(19) Koós, Á.; Solymosi, F. *Catal. Lett.* **2010**, *138*, 23−27.
(20) Huang, Y.; Zhou, X.; Yin, M.; Liu, C.; Xing, W. *Chem. Mater.* **2010**, *22*, 5122−5128.
(21) Tedsree, K.; Li, T.; Jones, S.; Chan, C. W. A.; Yu, K. M. K.; Bagot, P. A. J.; Marquis, E. A.; Smith, G. D. W.; Tsang, S. C. E. *Nat. Nanotechnol.* **2011**, *6*, 302−307.
(22) Solymosi, F.; Koós, Á.; Liliom, N.; Ugrai, I. *J. Catal.* **2011**, *279*, 213−219.
(23) Zhao, Y.; Deng, L.; Tang, S.-Y.; Lai, D.-M.; Liao, B.; Fu, Y.; Guo, Q.-X. *Energy Fuels* **2011**, *25*, 3693−3697.
(24) Bi, Q.-Y.; Du, X.-L.; Liu, Y.-M.; Cao, Y.; He, H.-Y.; Fan, K.-N. *J. Am. Chem. Soc.* **2012**, *134*, 8926−8933.
(25) Leadbeater, N. E.; Marco, M. *Chem. Rev.* **2002**, *102*, 3217−3274.
(26) McNamara, C. A.; Dixon, M. J.; Bradley, M. *Chem. Rev.* **2002**, *102*, 3275−3300.
(27) Mori, K.; Hanafusa, A.; Che, M.; Yamashita, H. *J. Phys. Chem. Lett.* **2010**, *1*, 1675−1678.
(28) Miguel-García, I.; Berenguer-Murcia, Á.; Cazorla-Amorós, D. *Appl. Catal., B* **2010**, *98*, 161−170.
(29) Deluga, G. A.; Salge, J. R.; Schmidt, L. D.; Verykios, X. E. *Science* **2004**, *303*, 993−997.
(30) Shin, W. C.; Besser, R. S. *J. Power Sources* **2007**, *164*, 328−335.
(31) Yadav, M.; Akita, T.; Tsumori, N.; Xu, Q. *J. Mater. Chem.* **2012**, *22*, 12582−12586.
(32) Mori, K.; Yamashita, H. *Phys. Chem. Chem. Phys.* **2010**, *12*, 14420−14432.
(33) Ruban, A.; Hammer, B.; Stoltze, P.; Skriver, H. L.; Nørskov, J. K. *J. Mol. Catal. A: Chem.* **1997**, *115*, 421−429.
(34) Judai, K.; Abbet, S.; Wörz, A. S.; Heiz, U.; Giordano, L.; Pacchioni, G. *J. Phy. Chem. B* **2003**, *107*, 9377−9387.
(35) Abild-Pedersen, F.; Andersson, M. P. *Surf. Sci.* **2007**, *601*, 1747−1753.